The Monte Carlo Method: Versatility Unbounded In A Dynamic Computing World
Chattanooga, Tennessee, April 17–21, 2005, on CD-ROM, American Nuclear Society, LaGrange Park, IL (2005)

The Use of Voxel-Based Human Phantoms in FLUKA

L. Pinsky and A. Empl
Physics Department
University of Houston
4800 Calhoun Blvd., Houston, TX 77204-5005 USA
anton.empl@cern.ch; pinsky@uh.edu

A. Ferrari
CERN and INFN & University of Milan
CERN
CH-1211, Geneva, Switzerland
alfredo.ferrari@cern.ch

G. Battistoni and P. Sala
INFN & University of Milan
Via Celoria 16, I-20133Milan, Italy
giuseppe.battistoni@mi.infn.it, paola.sala@cern.ch

F. Ballarini and A. Ottolenghi
INFN & University of Pavia
Via Bassi 6, I-27100 Pavia, Italy
francesca.ballarini@mi.infn.it, andrea.ottolenghi@mi.infn.it

Johannes Ranft
Physics Department
Siegen University
D-57068 Siegen, Germany
johannes.ranft@cern.ch

Alberto Fasso'
Stanford Linear Accelerator Center
2575 Sand Hill Road, Menlo Park, CA 94025
fasso@slac.stanford.edu

H. Paretzke and M. Zankl
GSF-National Research Center for Environment and Health
Ingolstadter Landstr. 1, D-85764 Neuherburg, Germany
paretzke@gsf.de, zankl@gsf.de

ABSTRACT

The FLUKA Monte Carlo code has been evolving over the last several decades and is now widely used for radiation shielding calculations. In order to facilitate the use of FLUKA in dosimetry and therapy applications, supporting software has been developed to allow the direct conversion of the output files from standard CT-scans directly into a voxel-based geometry for transport within FLUKA. Since the CT-scan information essentially contains only the electron density information over the scanned volume, to support Monte Carlo radiation transport calculations a separate method to obtain the specific compositions for each voxel individually is needed. We have developed a simple algorithm to assign tissues in the human body to one of four categories: soft-tissue, hard-bone, trabecular-bone and porous-lung. In addition we explore the problem of the path-length distributions in porous media like lung tissue and trabecular bone, where a detailed simulation of the actual micro-structure is impractical. One mechanism to accommodate this problem within FLUKA is based on the use of variable materials for the individual voxels in question. The potential materials for a given voxel are selected from a fixed set of choices based on the tissue type, the CT-scan measured density and a prior knowledge of the path length distributions. This paper represents the status of the work at approximately 6-months prior to the intended presentation, and additional work, including improved version of the material assignment algorithms as well as work on the simulation of transport through lung tissue are planned for inclusion in the actual oral presentation.

Key Words: Radiation Transport, Human, Voxel, Phantom, Monte-Carlo, Simulation

1 INTRODUCTION

Monte Carlo transport codes like FLUKA are useful for many purposes, and one of those is the simulation of the effects of radiation traversing the human body. In particular, radiation has been used in cancer therapy for a long time, and recently this has been extended to include heavy ion particle beams. This capability is also of interest to NASA because of the nature of the radiation environment in space.[1] While in space, the crew members' bodies are continually being traversed by virtually all forms of radiation. In assessing the risk that this exposure causes, heavy ions are of primary importance. These arise both from the external space radiation itself, as well as fragments that result from interactions during the traversal of that radiation through any intervening material including the body tissue itself. Thus the capability to characterize the details of the radiation field accurately within a human body subjected to such external "beams" is of critical importance.

In order to provide this capability by making use of the widest practical application of the known physics, the FLUKA Monte Carlo code has been extended over the last several years to include the ability to simulate heavy-ion interactions more completely.[2] Currently, FLUKA is available with internal event generators that are capable of simulating inelastic nuclear reactions down to an incident lab kinetic energy of ~100 MeV/A.[3] Work is in progress to extend the internal event generator capability all the way down to the reaction thresholds, as well as to update and improve the existing capabilities on a continuing basis as new data become available.

One common hurdle in the use of all Monte Carlo radiation transport codes is the difficulty of providing the detailed geometry information about the system to be modeled. This is particularly problematic when the object is as complex as the human body. The difficulty is multiplied by the requirement not only for an accurate positional geometric description, but also the absolute need to attach to that positional information the details of the composition and

density of the actual material. In cases where the human body is the object of the simulation, the technique of using information from CT-scans has been common, especially where the nature of the incident beam is restricted to electromagnetic radiation and electrons. This is because the primary information from a CT-scan is a measure of the local distribution of electron density in the object scanned. Raw CT-scan files are generally represented as scan layers of fixed thicknesses with data from individual cells within each sequential layer being given in raster pixel format. The three-dimensional volume element made up of each of these pixels in a given layer is referred to as a "voxel."

In order to be able to accept these raw CT-scan inputs, FLUKA has been modified to allow for the direct embedding of a region composed of these internal voxels within any normal FLUKA geometric description. So for example, one could embed a CT-scan-based voxel human phantom region within a spacecraft that was otherwise described using the normal FLUKA capabilities. Similarly, a CT-scan-based voxel phantom can be embedded in the external laboratory environment geometry description for simulation of accelerator-based exposures.

Unfortunately, by itself, a raw CT-scan is not as useful in providing a basis for the transport geometry when hadronic beams are applied due to the general lack of direct compositional information. This can be remedied if there is some external process whereby the composition can be associated with each individual voxel. In some cases, like the soft tissue in the human body, the use of a common global generic composition is a very good approximation. However, when dealing with the whole body or large fractions of it, this technique produces incorrect results because some organs, particularly bone and the lungs have both notably different compositions and porous structures.

2 ASSIGNING COMPOSITION

In order to address these issues, we have explored the development of an algorithm to distinguish bone and lung tissue from the other soft tissues within the body. The additional small problem of the existence of gas pockets, for example in the stomach and bowel, are easily included due to the very dramatic difference in density.

Our intention is to provide a compositional tag for each voxel that is either a generic "soft tissue," that is global for all soft tissue, or one of the special tissue types including hard bone, trabecular bone and porous lung. It should be emphasized that the actual measured densities will be used scaled to the generic composition assigned based on the x-ray cross sections, which are typically proportional to the electron density. For example, the density of each soft tissue voxel can still vary, even though the presumed elemental composition remains the same.

The challenges for bone and lung tissue are actually of two distinct kinds. First, there is the initial problem of simply distinguishing this tissue from the surrounding soft tissue. This is generally a pattern recognition problem which yields to well-know techniques that take advantage of density variations. Lung tissue is relatively easy to distinguish, but bone is more problematic. The thin "hard bone" shell that surrounds most human bone tissue is filled with an inner trabecular bone that is a combination of hard-bone filaments and a variety of different kinds of marrow. This composite trabecular bone tissue is typically unresolved on many large-

scale CT-Scans, and has an average density that can be similar to the surrounding soft tissue. However, the general property that it is internal to the hard-bone shell typically provides a handle on distinguishing it from the external soft-tissue. We have developed several software tools to facilitate the development of these algorithms.

In general the work reported here has been done using two separate sources for CT-scans. The first is a whole-body image of an adult male [2] that has been previously analyzed by hand to assign voxel by voxel the organ membership along with the corresponding material composition. The second image is that of trabecular bone and represents a 1.2 cm cubic volume entirely with the region of trabecular bone with a 40 μm voxel size. In this case, all voxels are identified either as entirely hard-bone or entirely interstitial marrow.[4]

Figure 1 shows the displays employed to develop the appropriate algorithms. Figure 1(a) contains the whole body image where the voxel densities of the slices shown have been displayed as a corresponding linear gray-scale. Figure 1(b) shows the same image processed by a simple density-based algorithm to distinguish the hard bone from soft tissue. Note that there is a histogram tool towards the top which displays the actual density profile for the vertical cross-hair line and a fit to that profile by the algorithm. The results are displayed for comparison in the image itself. One can see that the hard bone is easily distinguished from the soft tissue in a general sense. The major difficulties are with the boundary voxels and distinguishing the internal trabecular bone from general soft tissue.

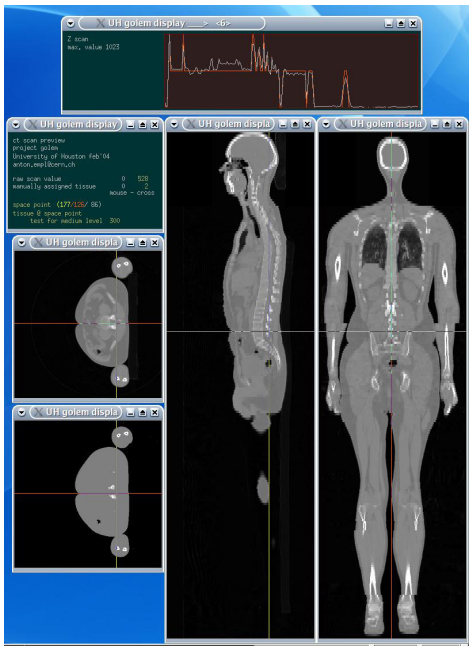

Figure 1(a)

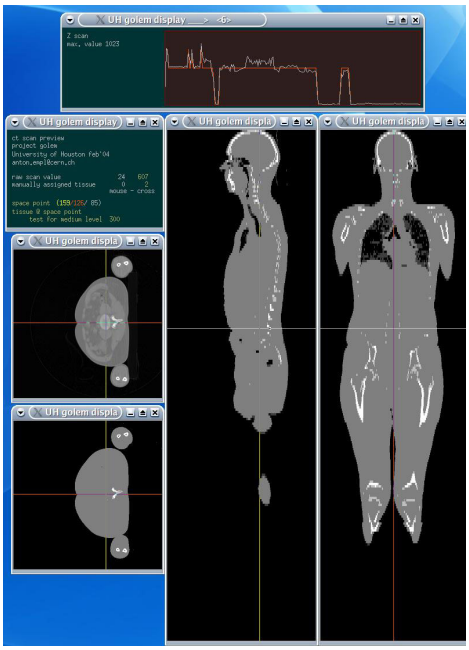

Figure 1(b)

Figure 1. Screen Shots are presented of the software tool developed to assess the performance of the tissue assignment algorithm. Figure 1(a) shows a slice from the “Golem” CT-scan where the raw density values are displayed on a linear brightness scale as pixels. Figure 1(b) shows the result of filtering this image with the simple threshold algorithm. Note the histogram tool that displays the raw data across the slice and the values from the

algorithm superimposed.

The boundary between hard bone and soft tissue can be problematic because the actual physical boundary between the outer hard-bone surface and the surrounding soft tissue generally occurs in the midst of a voxel rather than close to or along a voxel side. The current algorithm employs the simplest reasonable solution and assigns the voxel either as hard bone or soft tissue. A more complex solution that may be employed is similar to the one that has been developed to deal with the trabecular bone regions as discussed in the next section.

Figure 1(b) also shows that the lungs are easily distinguished from the surrounding tissue, and even the central region where the major pulmonary arteries and veins enter the lungs, the distinctions are fairly clear. The lung boundaries present the same challenge as does the bone boundary, and are amenable to the same solutions. These simple algorithms are subject to improvement, but given the level of success that has already been achieved by our methods; considerable progress has been made in getting the material properties into the Monte Carlo geometry inputs.

3 TRABECULAR BONE POROSITY

The porosity of trabecular bone and the lungs provides a separate distinct challenge. The problem stems from the fact that the details of porosity occur at a scale that is not practical to evaluate in large volume whole-body CT-scans. As such if the voxel is treated as possessing some mean density with a homogeneous composition, then all tracks traversing the voxel with the same trajectory-length in the voxel will see the identical material path-length in gm/cm^2. In reality, the pseudo-random porous nature of the material will actually give rise to a distribution of path-lengths. Further, in the case of trabecular bone, this distribution can also have a directional dependence. A similar problem was recognized by Wilson, et al.[5] in the treatment of the transport problem in fabric.

Several FLUKA runs were performed on the 40 μm resolution trabecular bone CT-scan image using rays to determine the actual path-lengths within the hard bone component of the trabecular bone. This particular example of trabecular bone possessed about 10% of its voxels as hard-bone with the remainder being treated as vacuum for our purposes here. Hard bone is taken to have a density of 1.920 gm/cm^2 and the path-length distributions are all given in terms of the gm/cm^2 of hard bone traversed per cm of total path-length traversed. The data are limited to rays with a minimum 0.5 cm path-length in the trabecular bone volume.

Figure 2(a) shows the path-length distribution for ~100,000 rays which are incident isotropically on the CT-scan volume. It is seen that there are essentially no rays that manage to avoid all hard-bone voxels, and the mean is about 0.1 gm/cm^2/cm. Figure 2(b) is an expanded view of the long path-length tail of the same distribution.

Figure 3(a) shows the result for another 100,000 rays, but for which the direction is strictly vertical, along the axis of the bone. Slightly more than 50% of these rays pass through the full 1.2 cm of trabecular bone without striking any hard bone voxels!.. This implies that strictly along the axis of the bone, the path-length variation is a very important feature for particle transport.

Figure 3(a) shows a similar set of rays, but where the angle with respect to the bone axis is distributed uniformly over a 100 mrad cone. However, note that even this modest angular deviation from the strict longitudinal axis causes a rapid reduction of this anomaly with the result tending towards the isotropic distribution with the virtual disappearance of the zero path-length rays.

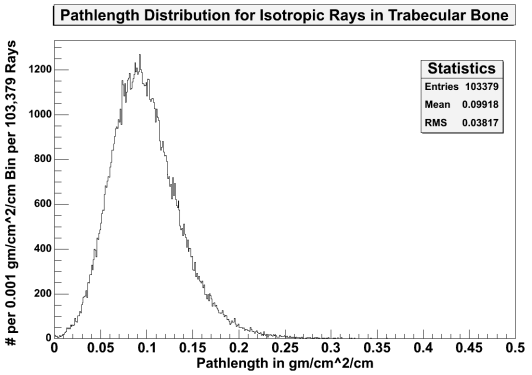

Figure 2(a)

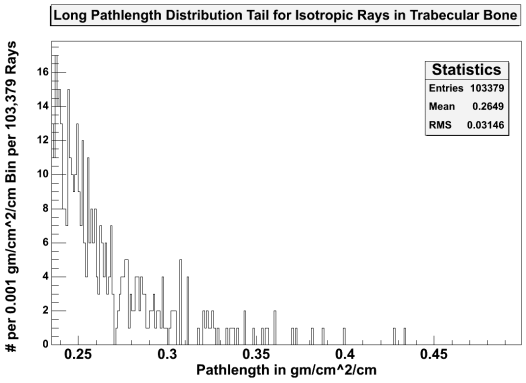

Figure 2(b)

Figure 2. This displays the path-length distributions in trabecular bone for an isotropic irradiation. All path-lengths included in the plot have a minimum 0.5 cm absolute length, and the results are plotted as gm/cm^2 of hard bone per actual cm of path-length. Figure 2(a) is an enlargement of the long path-length tail. The distribution fits a normal distribution quite well.

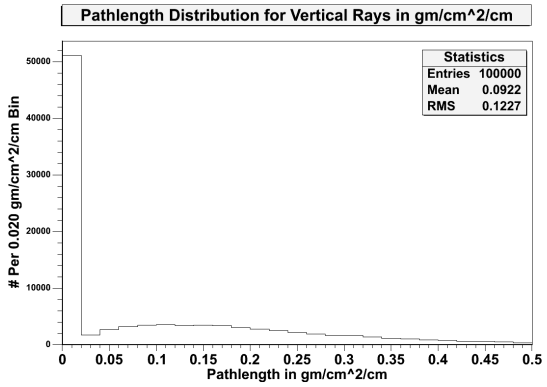

Figure 3(a)

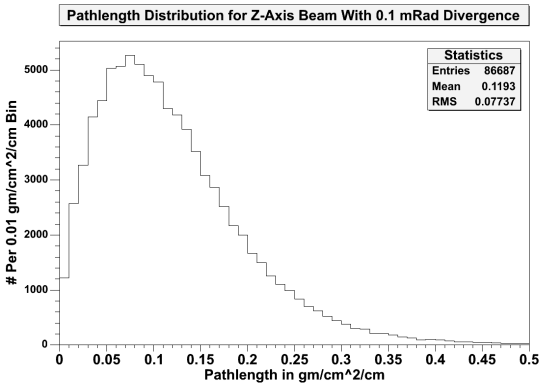

Figure 3(b)

Figure 3. This displays the path-length distributions similar to those of Figure 1, but for tracks incident along the longitudinal axis of the bone (the Z-axis) in our coordinate system. Figure 2(a), which is a plot for rays strictly parallel to the Z-axis, shows the surprising behavior of possessing a considerable peak at zero path-length. However, in contrast, Figure 2(b), which has its rays diverging from the Z-axis with this divergence spread uniformly over angle up to 100 m-radians, and the large zero path-length peak is entirely missing.

Figure 4 shows the result for a lateral beam (perpendicular to the bone axis) with no angular spread. A comparison with Figure 2(a) shows that the lateral path-length distribution is comparable to the general isotropic distribution.

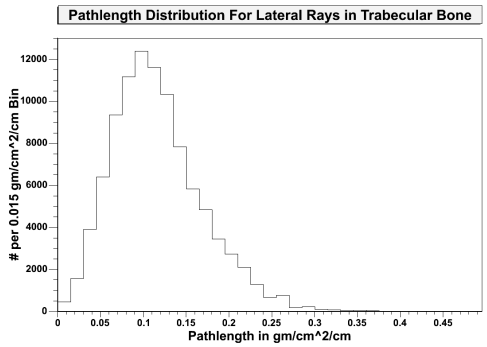

Figure 4

Figure 4. This plot shows the path-length distribution that results from an exposure to rays that are exactly parallel to one of the axes that is perpendicular (the reference to X-axis here is intended to be a generic axis perpendicular to the longitudinal axis of the bone). Like Figure 3(a), there is no divergence in the beam, but unlike that figure, there is no corresponding zero path-length peak.

Thus, it appears as if a strategy can be deployed wherein the path-length used is compensated by a normal distribution fit to the isotropic path-length distribution, with the provision that for particle directions that are very close to axial along the bone, a second distribution should be used that is a combination of (a) 50% no hard bone, and (b) 50% of twice the standard isotropic path-length distribution.

To implement this strategy, rather than vary the actual path-length, the mechanism to be employed within FLUKA will be to provide for a new kind of material that has a variable material type. This is more practical than trying to employ a variable density due to the need to have pre-calculated cross section related information for each separate density of material. Thus, when a particle enters such a medium the program will select the material type to be used for that particle randomly from a distribution function that reflects the actual density of the voxel as determined from the CT-scan as well as the relative densities of the different materials known to be representative of that particular type of tissue. For example, in trabecular bone, the voxels will be modeled with a combination of hard bone and marrow as two alternative tissue types, The probability that either will be used will be determined by the relative ratio of the densities with respect to the actual average measured density for that voxel. For lung tissue, the two alternative tissue types would be blood and air. It is possible to consider situations where more than two alternative material types might be used, however, for the human phantom problem, it is reasonable to model these most problematic cases with just two alternatives. This approach will allow the effect of the porosity of the medium to be more properly simulated with respect the net effect on a traversing beam of charged particles in terms of the spreading of the energy loss effects as well as the other interaction probabilities.

4 MODELING POROUS LUNG TISSUE

Lung tissue poses the same kind of problems for beam transport calculations as trabecular bone, with one significant difference. The scale of the porosity of lung tissue changes substantially from one location to another within the volume of the lung. That is, the fraction of the volume of dense to less dense material varies significantly from one region to the next. However, the calculational method that we have adopted for treating the micro-porosity problem generally lends itself nicely to an alternative solution for lung tissue. We assume that the density of the internal lung tissue voxels represents the fraction of dense to less dense of the known material choices (blood and air. Thus one only need tailor the ratio used in a particular voxel to determine the material choice to be made each time a particle approaches a particular voxel by the relative difference between the values of the density assuming it is only composed of air and blood. For example, If a particular internal lung voxel has a density greater than the value for air in that same CT-scan, but only 25% of the gap between air and blood, then the probability that blood will be used for the entire voxel is only 25% and the corresponding probability for using air for the entire voxel volume would be 75%.

5 CONCLUSIONS

Work is proceeding on developing tools to employ FLUKA in applications where detailed simulations of the effects in specific human subjects are desired. CT-scans can be used to supply individual geometry information as an input to the code, with ancillary tools being employed to supply the compositional information from generic sources, which is added to the geometric and density information present in the CT-scan data. The specific problem of accurately predicting the effects of transport through porous media has been solved by introducing variable material media types into FLUKA.

6 ACKNOWLEDGMENTS

We would like to acknowledge the use of the so-called “Golem” whole-body CT-scan data set along with the version that resulted from the efforts of Laura De Biaggi in her detailed voxel by voxel assignment of individual organs to that data set and the similar efforts of Maria Zankl. We are also grateful to Professor Gemunu Gunaratne of the University of Houston for providing access to the trabecular bone CT-scan employed as well as for his efforts in producing graphic images of the CT-scan. Finally, we gratefully acknowledge the permission of Professor Michael A.K. Liebschner of the Bioengineering Department of Rice University to use the trabecular bone CT-scan which Professor Gunaratne had obtained from him originally. This work was partially supported by the EC (contract no. FI6R-CT-2003-508842, "RISC-RAD"), NASA (Contracts NAG8-1901 and NAG8-1658) and the Institute for Space Systems Operations at the University of Houston.

7 REFERENCES

1. V. Andersen F. Ballarini G. Battistoni, M. Campanella, M. Carboni, F. Cerutti, A. Empl, A. Fassò, A. Ferrari, E. Gadioli, M.V. Garzelli, K. Lee, A. Ottolenghi, M. Pelliccioni, L.S. Pinsky, J. Ranft, S. Roesler, P.R. Sala and T.L. Wilson, The FLUKA code for space applications: recent developments. Adv. Space Res, in press (2004).

2. F. Ballarini, M. Biaggi L. De Biaggi, A. Ferrari, A. Ottolenghi, A. Panzarasa, H.G. Paretzke, M. Pelliccioni, P. Sala, D. Scannicchio and M. Zankl, Role of shielding in modulating the effects of Solar Particle Events: Monte Carlo calculation of physical and "biological" dose in different organs. Adv. Space Res., in press (2004).

3. A. Fassò, A. Ferrari, S. Roesler, P.R. Sala, F. Ballarini, A. Ottolenghi, G. Battistoni, F. Cerutti, E. Gadioli, M.V. Garzelli, A. Empl, J. Ranft, The physics models of FLUKA: status and recent developments CHEP-2003-MOMT005, Jun 2003. 10pp. Talk given at 2003 Conference for Computing in High-Energy and Nuclear Physics (CHEP 03), La Jolla, California, 24-28 Mar 2003. Published in eConf C0303241:MOMT005,2003 e-Print Archive: hep-ph/0306267 (2003).

4. Gunaratne, G. and Leibschner, M., Private Communication (2004).

5. J.W. Wilson, J. Tweed, C. Zeitlin, M.-H.Y. Kim, B.M. Anderson, F.A. Cucinotta, J. Ware, A.E. Persans, Shuttle Spacesuit: Fabric/LCVG Model Validation, Paper Number 01ICES-2372, Society of Automotive Engineers (2001).